Rectifier Effect in an Atmospheric Model with Daily Biospheric Fluxes: Impact on Inversion Calculation

Misa Ishizawa[1,2*], Douglas Chan[2], Kaz Higuchi[2], Shamil Maksyutov[3], Chiu-Wai Yuen[1], Jing Chen[1] and Douglas Worthy[2]

[1]University of Toronto, Toronto, Ontario M5S 3G3, Canada
[2]Atmospheric Science and Technology Directorate, Environment Canada, Toronto, Ontario M3H 5T4, Canada
[3]National Institute for Environmental Studies, Tsukuba 305-8506, Japan

[*] Corresponding author.
e-mail: misa.ishizawa@ec.gc.ca

Abstract

Atmospheric CO_2 measurements show strong synoptic variability. To understand the contribution of the synoptic signals on atmospheric CO_2 inversion, we simulate the cases of biospheric fluxes with and without synoptic variations (referred to as 'Synoptic' and 'Reference', respectively) using an atmospheric transport model, and then perform inversion analyses with these biospheric CO_2 concentration fields.

Results show the monthly and annually averaged CO_2 concentration anomalies (Synoptic – Reference) are functions of the distance from the continental biospheric source regions. Remote sites (like Mauna Loa) show averaged monthly amplitude of ~0.2ppm, while continental sites show averaged monthly amplitudes of 1-2ppm with maximum monthly amplitudes up to 7ppm. Spatial scales of these monthly mean synoptic anomaly patterns may exceed 1000km. These CO_2 concentration patterns are the results of the interaction of the synoptic CO_2 flux field and atmospheric transport, and may be referred to as the synoptic Rectifier Effect.

Inversion CO_2 fluxes for 1992-1995 are obtained using biospheric background fields with and without synoptic biospheric flux variations. The maximum magnitude differences in estimated monthly flux for land and ocean regions are ~0.4 and ~0.2 $GtC \cdot month^{-1}$ respectively. The average land sink increases by 0.19 $GtC \cdot yr^{-1}$ while the average ocean sink decreases by 0.30 $GtC \cdot yr^{-1}$.

1. Introduction

Inversion of atmospheric CO_2 concentration (mixing ratio) measurements to estimate spatial and temporal distributions of CO_2 sources/sinks has become a popular scientific endeavour (e.g., Rayner et al., 1999; Gurney et al., 2002; 2004; Baker et al., 2006). This scientific activity constitutes an important investigation in trying to understand the processes and mechanisms controlling CO_2 sources/sinks distribution within the global carbon cycle, both in time and space. However, we are faced with an under-determined problem because we do not have sufficient number of observations to constrain the spatial-temporal distribution of CO_2 fluxes to the atmosphere uniquely (Enting, 2002). In order to overcome this deficiency of available atmospheric CO_2 measurement, it has been a typical practice to include some *a priori* information about the carbon cycle system so that the inverse solution would be consistent with our prior knowledge of the system.

In this Bayesian synthesis inverse approach (Tarantola, 1987; Rayner et al., 1999) used here, we generate an atmospheric background CO_2 concentration field by assigning a CO_2 surface flux distribution for an atmospheric transport model. The flux distribution, both in time and space, includes contributions from fossil fuel combustion, ocean and terrestrial biosphere. These background values are subtracted from the observed CO_2 concentrations at individual monitoring sites, with the residual allocated in an optimized way to various source regions as net CO_2 fluxes in accordance with a set of response function. Each response function represents the resultant temporal evolution of CO_2 concentration at a measurement site in response to the release of a unit CO_2 flux from a basis region. A response function is essentially a "source-receptor" relationship.

In TransCom 3 Level 1 (Gurney et al., 2002) and TranCom 3 Level 2 (Gurney et al., 2004), global distributions of annual mean and monthly mean carbon sources and sinks were estimated, respectively, averaged over the period 1992 to 1996. In both studies, net carbon fluxes were estimated for 11 land and 11 ocean regions. For the background field, fluxes from the 1990 and 1995 fossil fuel emissions (Andres et al., 1996; Brenkert, 1998), seasonally-varying air-sea flux (Takahashi et al., 1999) and an annually balanced monthly net CO_2 flux from a global terrestrial ecosystem model (the CASA model, Randerson et al., 1997) were used. In this study, we investigate the impact on inverse flux estimates of using annually-balanced monthly net terrestrial biospheric flux in generating the background field.

Chan et al. (2004) showed that the atmosphere-biosphere exchange of CO_2 is accomplished by processes on various time scales. They identified the significance of synoptic and mesoscale processes in transporting biospheric CO_2 flux signal into the troposphere. (Typical synoptic scale processes include cyclones and anticyclones with horizontal spatial scale of ~1000km and time scale of ~5-10 days. Typical mesoscale processes include thunderstorms and rainbands with horizontal spatial scale of ~10-100km and time scale of ~0.1-1 day.) The atmosphere-biosphere interaction on a daily time scale (by synoptic and mesoscale processes including fronts and cyclones) was shown to be important, with possible impact on Rectifier Effect (Denning et al., 1995; 1996a, b). The Rectifier Effect is typically defined as the annual time-mean spatial CO_2 concentration gradient in the atmosphere caused by a covariance between the annually neutral biospheric CO_2 flux and the atmospheric transport. For example, the seasonal Rectifier Effect in the typical transport model is the annual time-mean spatial CO_2 concentration gradient in the atmosphere caused by the monthly varying biospheric CO_2 flux. However, other rectification processes are possible, e.g. Gurney et al., (2005) investigated the possible rectification from seasonal variations in the fossil fuel sources.

In this study, using the NIES (National Institute of Environmental Studies) atmospheric transport model (Maksyutov and Inoue, 2000) and Biome-BGC (BioGeochemical Cycles) biospheric model (Thornton et al., 2002; Fujita et al., 2003), the contribution of daily atmosphere-biosphere interaction to the monthly to annually averaged CO_2 concentrations are characterised spatiotemporally by comparing the model simulated CO_2 concentrations with CO_2 fluxes varying on daily versus monthly time steps. Then, the effects of the daily CO_2 flux and atmospheric transport on time-dependent inverse flux estimates are investigated by comparing inversions with daily and monthly biospheric CO_2 fluxes.

2. Method

The method used in this study is a variation of the TransCom 3 Level 2 (T3L2) protocol (Gurney et al. 2000). The necessary change is the simulation of daily biospheric fluxes to capture as much as possible the synoptic atmosphere-biosphere interaction in the forward simulation. The models used in this study are the NIES atmospheric transport model and the Biome-BGC ecosystem model.

The NIES model (Maksyutov and Inoue, 2000) uses NCEP (National Centers for Environmental Prediction) reanalysis meteorology (Kalnay et al., 1996) to transport the atmospheric CO_2 concentrations resulting from the surface CO_2 fluxes. The model domain uses the latitude-longitude horizontal grid with a resolution of 2.5° x 2.5°. Vertically, the model has 15 sigma levels ranging from 0.985 to 0.065 (~0.15km to ~20km in altitude, exact height depends on surface pressure). Time step in the model is 2 hours. The advection scheme is semi-Lagrangian with mass adjustment to conserve tracer mass. The planetary boundary layer (PBL) height in the model is specified with the monthly mean climatological PBL heights (from the Data Assimilation Office at NASA's Goddard Space Flight Center). Besides the advection by vertical wind, two vertical mixing processes in the model are: (1) turbulent diffusion which is temperature dependent (stability function), and (2) cumulus convection derived from the humidity, temperature, and wind fields (see Appendix A for details of vertical mixing processes). Although the PBL is specified with the climatological mean monthly values, these other vertical mixing processes can approximately represent the synoptic scale transport processes resolvable in the NCEP meteorology (particularly above the PBL) within a transport model.

The Biome-BGC model (Thornton et al., 2002) computes the daily ecosystem fluxes including NPP (net primary production), HR (heterotrophic respiration) and NEE (net ecosystem exchange) in response to atmospheric forcing such as temperature, humidity, precipitation and radiation. (See Fujita et al. (2003) for a detailed description of the model.) The model resolution is 1° x 1°, with a time step of 1 day. The meteorological forcing is the NCEP reanalysis meteorology. By using the same NCEP reanalysis meteorology in the Biome-BGC and NIES models, the CO_2 fluxes and CO_2 transport are mutually consistent. For example, under a cloudy cyclonic system, the solar radiation reaching the surface is reduced leading to the reduction of photosynthesis, resulting in the relatively enhanced CO_2 flux into the atmosphere; in turn this enhanced CO_2 flux is transported higher into the atmosphere by the more convective vertical motion. Thus this model can capture the synoptic scale interaction between the atmosphere and the biosphere inherent in the NCEP data. As there is no constraint requiring these daily atmosphere-biosphere interactions to average to zero on the monthly or longer time scales, these interactions might have contributions to the monthly and annual CO_2 concentration fields and consequently on inversion flux estimates based on these CO_2 concentration fields. These effects are examined in the following forward and inverse modelling.

2.1. Forward simulation strategy

2.1.1 Daily and monthly CO_2 fluxes:

The global 1° x 1° daily biospheric fluxes including NEE and NPP are simulated with the Biome-BGC model and the NCEP meteorology for the 10-year period from 1990-1999. The daily NEE fluxes are adjusted to be annually neutral at every grid point each year. The adjustment consists of applying a minor constant correction to HR throughout the year. This adjusted NEE flux is referred to as the 'daily NEE flux.' Next the daily NEE fluxes for each individual month over the 10 years are averaged and are referred to as the 'monthly mean NEE fluxes.' Thus the monthly mean flux is comparable to the CASA flux used in the TransCom experiments.

2.1.2 Transport of atmospheric CO_2 concentrations:

Transport simulations consist of two cases referred to as the Reference and Synoptic Cases.
(i) Reference Case: Simulate the transport of CO_2 for 10 years with the NIES model using NCEP winds from 1990-1999 and the monthly mean NEE flux repeated each year.
(ii) Synoptic Case: Simulate the transport of CO_2 for 10 years with the NIES model using NCEP winds from 1990-1999 and the daily NEE flux from 1990-1999.

For the evaluation of model performance, the modeled atmospheric CO_2 concentrations are shown in comparison to the observations at three sites in Appendix B. To examine the effects of the synoptic atmosphere-biosphere interaction, the presentation of results will focus on the differences in the CO_2 concentrations between the two cases.

2.2. Inversion strategy

To quantify the effects of the synoptic atmosphere-biosphere interaction on inversion estimates, we repeat the time dependent (for the period from 1992-1995) TransCom 3 monthly inversion (Baker et al., 2006) with the Biome-BGC monthly mean NEE fluxes (Reference Case, replacing the CASA fluxes used by TransCom 3) and compare the results to the inversion estimates obtained from the CO_2 background field generated by the daily NEE fluxes (Synoptic Case). In this study, we used the same set of monthly station observed atmospheric CO_2 concentration (78 sites) and their associated uncertainties from *GLOBALVIEW-*CO_2 (2000) and Bayesian inversion program by Gurney et al. (2000). GLOBALVIEW is a data product that interpolates CO_2 measurements by continuous analyzer or by sub-weekly flask samples into monthly interval, with an extrapolation procedure to fill the data gaps (*GLOBALVIEW-*CO_2, 2000). The presentation of results will focus on comparing the differences in the CO_2 flux estimates between the Reference and Synoptic cases.

3. Results and Discussion

3.1. Temporal Evolution

In the inversions, typically monthly-averaged atmospheric CO_2 concentration data from the forward simulations are used. Therefore the monthly time series of the modeled CO_2 concentrations at a number of selected sites are examined in this section. The results shown are the difference of the monthly-averaged CO_2 concentration between the Synoptic Case and the Reference Case (referred to as 'synoptic CO_2 concentration anomalies' or simply 'CO_2 anomalies'). Thus the monthly-averaged CO_2 concentration differences or anomalies represent the transported signal from the difference between the biospheric daily CO_2 fluxes and the biospheric monthly CO_2 fluxes. In short, this difference between the biospheric daily CO_2 fluxes and the biospheric monthly CO_2 fluxes will be referred to as the 'synoptic biospheric flux anomalies' or simply 'flux anomalies'. By definition, these synoptic biospheric flux anomalies have daily flux variability but zero annual totals at every point in the model.

The results are strongly dependent on the relative distance to the synoptic source/sink regions. Figure 1 shows the locations of the sites covering different cases ranging from within the source region to far remote sites (site descriptions are summarized in Table 1) where the time series of the CO_2 anomalies are shown in Fig. 2.

Far from the continental synoptic biospheric flux anomalies, sites like Mauna Loa (19.53°N, 155.58°W) and Cape Grim (40.68°S, 144.68°E) (Figs. 2a and 2b) have small monthly synoptic CO_2 concentration anomalies. The maximum monthly CO_2 anomaly amplitudes in the 10-year period are 0.67 ppm at Mauna Loa and 0.4 ppm at Cape Grim. Their 10-year mean monthly anomaly amplitudes are 0.17 ppm at Mauna Loa and 0.11 ppm at Cape Grim. At these remote sites, monthly averaging of the CO_2 concentration effectively removes the transported signal from the synoptic biospheric flux anomalies.

Another group of background sites are characterized as being near the continental synoptic biospheric flux anomalies such as Alert (82.45°N, 62.52 °W), Estevan Point (49.38°N, 126.55°W), Sable Island (43.93°N, 60.02°W) and Ryori (39.03°N, 141.83°E). The synoptic CO_2 concentration anomalies evolutions at these sites are shown in Figs. 2c-2f. The maximum monthly anomaly amplitudes in the 10-year period are 2.2 ppm at Alert, 2.1 ppm at Estevan Point, 4.1 ppm at Sable Island and 2.1 ppm at Ryori. Their 10-year mean monthly CO_2 anomaly amplitudes are 0.38 ppm at Alert, 0.36 ppm at Estevan Point, 0.63 ppm at Sable Island and 0.44 ppm at Ryori. Sable Island shows the strongest monthly variations in this group of stations for both the maximum and average monthly amplitudes. While Ryori and Sable Island are at similar distances downwind from the Asia and North America continents respectively, the Sable Island monthly CO_2 anomalies are larger than at Ryori. The synoptic atmosphere-biosphere interaction on the monthly timescale at the east coast of North America is stronger than at the east coast of Asia. This result is consistent with the fact that, in the ecosystem map used in the Biome-BGC model, Eastern North America mainly consists of forest, while East Asia has grassland; the Biome-BGC results show that the productivity in Eastern North America is larger than that of East Asia.

The locations with the largest monthly-averaged synoptic CO_2 concentration anomalies are the continental sites. Fraserdale (49.88°N, 81.57 °W) and Hegyhatsal (46.95°N, 16.65°W) are examples of such sites (Figs. 2g and 2h, respectively). The monthly CO_2 anomalies have maximum amplitudes of 4.6 ppm at Fraserdale and 6.3 ppm at Hegyhatsal; while the average monthly magnitudes are 1.2 ppm at Fraserdale and 1.7 ppm at Hegyhatsal. These amplitudes are about one order of magnitude larger than those at the remote locations like Mauna Loa and Cape Grim. Europe in particular is a region with frequent large CO_2 anomalies. The correlation analyses (not shown) of the synoptic biospheric flux anomalies to the synoptic CO_2 concentration anomalies at these continental sites show no significant correlations. This indicates that the synoptic CO_2 concentration anomalies are not strongly dependent on the local synoptic biospheric flux anomalies but are the result of the interaction of transport and flux/concentration.

In Fig.2, the following characteristics are evident at each site. They all have strong monthly and inter-annual variations. Occasionally, the CO_2 anomalies have longer durations of a few months. There is no apparent seasonal pattern in the signs of the CO_2 anomalies; they may be positive or negative throughout the years.

3.2. Spatial Distribution

For some examples of the spatial CO_2 patterns, the global patterns of the monthly-averaged surface CO_2 anomalies for January to December 1992 are shown in Fig. 3. The CO_2 anomalies have a wide range of spatial scales, from hundreds to thousands of kilometers. These CO_2 anomalies range from -5 to 7 ppm. The stronger CO_2 anomalies are typically centred on land and persist for one month or so. Occasionally the CO_2 anomalies persist for longer periods. For example, a strong negative CO_2 anomaly with large spatial extent over the Ural mountain region persists from January to March, and a strong positive CO_2 anomaly in almost the same area persists from July to September. In fact, this area has strong CO_2 anomaly patterns throughout the 10 years of model simulation, reflecting the strong covariance of the atmospheric transport and the synoptic biospheric flux anomalies.

On the annual time scale, the spatial patterns of the annually averaged synoptic CO_2 concentration anomalies for 1992 and 1993 are shown in Fig. 4 as examples. The differences between these two years represent typical inter-annual variations. Even when averaged annually, some anomaly patterns remain in the surface CO_2 concentration field. These CO_2 deviations range from -1 to 1.5 ppm. The spatial patterns are similar to the monthly CO_2 anomaly fields with strong anomalies centred over land regions. There are strong inter-annual variations in the annual patterns. These annual CO_2 anomaly patterns represent the time-mean spatial CO2 concentration gradient in the atmosphere resulting from the covariance of the CO_2 concentrations from the synoptic CO_2 flux anomalies and the atmospheric transport. Therefore it may be referred to as the synoptic Rectifier Effect, analogous to the seasonal Rectifier Effect (Denning et al., 1995) identified for the covariance of the CO_2 concentrations from the monthly mean CO_2 fluxes and transport. A note of caution is required here. Since this model may not fully capture all the synoptic and sub-synoptic processes in the atmosphere and the biosphere, the results presented here may only be considered an approximation of the synoptic Rectifier Effect.

These results show the possible spatial and temporal range of atmospheric CO_2 variations in the biospheric background CO_2 concentration field with daily NEE fluxes compared to the standard biospheric background with monthly NEE fluxes.

3.3. Inversion

Using the biospheric fluxes from the Reference Case and Synoptic Case, we can obtain two biospheric backgrounds usable in inversions. The biospheric background from the Synoptic Case represents the CO_2 field with the Biome-BGC daily NEE fluxes. The inversion result using this biospheric background is referred to as the Synoptic Inversion. The biospheric background from the Reference Case represents the CO_2 field with the Biome-BGC monthly mean fluxes. The inversion result using this biospheric background is referred to as the Reference Inversion. The inversion procedure follows closely the time dependent inversion method for the monthly inversion of T3L2 (Baker et al. 2006). The main difference between the Reference Inversion and T3L2 is that the Reference Inversion in this study uses the Biome-BGC monthly mean fluxes, while T3L2 used the CASA monthly fluxes. This substitution is to ensure better comparability to the Synoptic Inversion. The CASA monthly fluxes mutually consistent with NCEP meteorology for different years required by the Synoptic Case are not available from TransCom for this study.

The period of inversion in this study is from 1992 to 1995. The biospheric background for the Reference Inversion is produced with the monthly mean NEE fluxes according to T3L2. The biospheric background for the Synoptic Inversion is generated with the daily NEE fluxes. Thus, the synoptic biospheric background for year 'n' is produced by releasing the daily NEE fluxes generated by the NCEP meteorology of year 'n' into the transport model and integrated using the NCEP winds from years n, n+1 and n+2. Since the flux and transport vary inter-annually in the Synoptic case, thus the 'interannual variations in the rectification' is also captured in the Synoptic case but not in the Reference case. The response functions are the same in both inversions to highlight the effects of the synoptic biospheric background on inversion results. Thus, monthly response functions are generated using the 10-year annual mean spatial distributions of NPP for the different land regions with atmospheric transport driven by the 1993-1995 NCEP meteorological data. Note it is worthwhile in future studies to examine the possible difference in inter-annual inversion results if the response functions include spatiotemporal variations in CO_2 flux patterns and inter-annual variations in the wind transport.

The monthly results from the two inversions for the 11 land and 11 ocean regions defined by TransCom 3 (See Fig. 1) are shown in Figs. 5 and 6 respectively. For the land regions, the monthly differences of the estimated fluxes between the Synoptic Inversion and the Reference Inversion vary with time and regions. The maximum magnitude of the differences is ~0.4 GtC $month^{-1}$. Also, there are periods when the differences have the same sign for a few months. The region with the most frequent and significant differences is Europe. This region was noted above to have large variability from the synoptic flux forcing. Other regions have slightly smaller inverse flux differences. The differences have monthly and inter-annual variations in most regions.

The ocean regions have smaller monthly differences (~0.2 GtC $month^{-1}$ or less) between the two inversions. Even though the only difference for the two inversions is a change in the biospheric background field, the inversion finds a 'best' solution with changes in the oceanic sources/sinks. Many ocean regions exhibit the monthly fluctuating differences similar to the land regions, except one ocean region (South Pacific).

The monthly fluxes are summed to yield annual inverse fluxes. The results for the 11 land and 11 ocean regions are shown in Figs. 7 and 8 respectively. The uncertainties in the annual flux estimates for the Reference Inversion are also shown in the figures; the uncertainties are very similar for the Synoptic Inversion and are omitted in the monthly results to maintain the clarity of the figures. The results show that annually there are differences among the regions. Figure 7 shows that the land regions Tropical Africa and Australia have minimal differences between the two inversions. The other land regions show larger differences and more temporal variability, including Europe which displays differences throughout the time period. The ocean regions in Fig. 8 display a similar range of differences between the two inversions. However, as noted above, South Pacific shows persistent and the largest differences of the same sign during the period. The difference between the two inversions can be as large as 0.5 GtC yr^{-1}. This may be a reflection of the poorly constrained nature of the region.

The annual results for all the land and ocean regions are summed to yield a global inversion flux estimate for each year. The results are summarized in Table 2. For the Reference Inversion, the results show large inter-annual variability for both land and ocean. The ranges of variation are 3.05 GtC yr^{-1} for land, 2.03 GtC yr^{-1} for ocean and 2.86 GtC yr^{-1} for the total (land + ocean). By including the synoptic biospheric variations, the inversion results show larger inter-annual variations for both land and ocean. The ranges are 3.39 GtC yr^{-1} for land, 2.26 GtC yr^{-1} for ocean and 2.83 GtC yr^{-1} for the total. These results represent 11% increases for both land and ocean, but a 1% decrease for the total.

For the individual years, there are large changes in fluxes both in magnitude and percentage. The largest difference in the land flux is 0.44 GtC yr^{-1} in magnitude (1993) and 22% in percentage (1993). The largest difference in the ocean flux is 0.48 GtC yr^{-1} in magnitude (1993) and 37% in percentage (1993). For the total of land and ocean, the largest difference is 0.16 GtC yr^{-1} in magnitude (1995) and 7% in percentage (1995). The pattern of increment of uptake for land and reduction of uptake for ocean persists throughout this 4-year period. The average land sink increased by 0.19 GtC yr^{-1} and the average ocean sink decreased by 0.30 GtC yr^{-1}.

Another overall measure of the difference from neglecting the synoptic variability in the biospheric background fluxes (referred to as between-methods difference) can be represented by the root mean square of the monthly differences of flux estimates between the two inversions. The results for the 22 regions are shown in Table 3. For comparison,

Table 3 also included the posterior uncertainties (mean of the Synoptic and Reference cases) for this study, as well as the ‘within-model’ uncertainties and ‘between-model’ uncertainties from Gurney et al. (2004). The posterior uncertainties in this study are similar to the ‘within-model’ uncertainties, indicating that the uncertainties are comparable (some of the differences between the posterior uncertainties of this study and the TransCom “within’ uncertainties might be the result of the inversions with different CO_2 observation sites, different time period of inversion, cyclo-stationery compared to time-dependent, and different biospheric fluxes). The region with the largest between-methods difference (1.65 GtC yr^{-1}) is Europe, the region with strong synoptic variations compared to the Reference case. This between-methods difference is about 4 times larger than the other uncertainties in Table 3. The other regions with about 2 times larger between-methods difference than the other uncertainties are Boreal North America, Temperate North America, Boreal Asia and Northern Ocean. These regions seem to be strongly influenced by the strong mid to high latitude continental synoptic forcing. The remaining regions show between-methods differences comparable to the other uncertainties.

4. Conclusions

The sparseness of CO_2 concentration observations makes atmospheric CO_2 inversion an under-constrained problem. The Bayesian inversion commonly used for CO_2 inversion includes many assumptions and approximations. Each assumption or simplification introduces uncertainties in the inversion results. This study examined the approximation that the biospheric fluxes have a smooth monthly variation. The spatiotemporal effects of sub-monthly or synoptic biospheric variations were studied by using the NIES transport model to simulate the cases of biospheric fluxes from the Biome-BGC model with and without synoptic variations. Then Bayesian inversion analyses were performed to estimate the effects of the synoptic atmosphere-biosphere interaction on regional flux estimates.

The spatiotemporal characteristics of the synoptic atmosphere-biosphere interaction were computed from the difference between the two simulations. Temporally, the synoptic biospheric flux anomalies did not average to zero and were present in the monthly and annually averaged atmospheric CO_2 concentrations. The synoptic CO_2 anomalies showed strong monthly and inter-annual variability. The magnitude of the synoptic CO_2 concentration anomalies was shown to be a strong function of the distance from the continental biospheric source regions.

On the monthly time scale, a remote site like Mauna Loa showed averaged monthly amplitude of 0.2 ppm with maximum amplitude of 0.7 ppm. Coastal sites showed averaged monthly amplitudes of 0.4-0.6 ppm, with maximum amplitudes of 2-4 ppm. Continental sites showed averaged monthly amplitudes of 1-2 ppm with maximum monthly amplitude exceeding 6 ppm. Spatially, the monthly CO_2 anomaly patterns with amplitudes up to ~7 ppm were shown to have typical length scales from a few hundred to a thousand kilometers. The CO_2 anomalies were centred over land regions. On the annual time scale, the spatial patterns were similar to the monthly patterns but the maximum CO_2 anomaly amplitude was reduced to ~1.5 ppm. These simulated synoptic CO_2 anomaly patterns were the results of the interaction of the synoptic CO_2 anomalies field and atmospheric transport, and were defined as the synoptic Rectifier Effect.

Two sets of inversion CO_2 fluxes were obtained following the TransCom3 level 2 time dependent method using biospheric background fields with and without synoptic biospheric flux variations. The 22-region monthly inversions were performed for the years 1992 to 1995. Comparisons showed that the synoptic Rectifier Effect on inversion varied in space and time. Monthly inversion differences were larger for the land regions than for the ocean regions. The maximum magnitude of the differences was ~0.4 GtC month^{-1} for the land regions and ~0.2 GtC month^{-1} for the ocean regions. In the 4 years of inversion results, the Synoptic Inversion showed 11% greater range of inter-annual variations for the annual land and ocean fluxes compared to the Reference Inversion.

These results are dependent on the models used. There are numerous approximations that could affect the simulation results of the synoptic interaction between the biosphere and atmosphere. These approximations include: prescribed PBL and low spatial resolution in the transport model, low temporal resolution in the NCEP meteorological data, and the lack of diurnal variation in the biospheric fluxes from the Biome-BGC model. Other important factors in the simulation of the atmosphere-biosphere interaction include the accuracy of the synoptic biospheric flux simulation, and the accuracy of the NCEP wind field data. Inversion results could be influenced by factors including coarse model resolution in space and time, observational data (quality, space-time resolution and processing). Capturing more atmosphere-biosphere interactions including the synoptic variations of the PBL and sub-synoptic scale interactions might result in a stronger synoptic Rectifier compared to this study. If the atmosphere-biosphere interactions are adequately simulated in the model and represent a more realistic state of the atmospheric CO_2 spatiotemporal distribution, then the results of this study suggest that properly designed inversion procedure may yield improved flux estimates by the inclusion of the synoptic atmosphere-biosphere interactions.

5. Acknowledgments

We thank Christian Rödenbeck for helpful comments on this manuscript. We are grateful for the constructive comments and suggestions by the two anonymous reviewers on our submission which have greatly helped to improve this manuscript. This work is partially funded by the Canadian Foundation for Climate and Atmospheric Sciences.

Appendix A

Two vertical mixing processes are represented in the model: (1) turbulent diffusion which is temperature dependent (stability function), and (2) cumulus convection derived from the humidity, temperature, and wind fields.

A.1. Turbulent diffusion

Below PBL top, the turbulent diffusivity is set to constant value of 40 m^2 s^{-1}. Above PBL, the turbulent diffusivity (K) is calculated using local stability function following Hack et al. (1993):

$$K = l^2 \cdot S \cdot F_S(Ri), \tag{A1}$$

where

$l = 30\ m$: mixing length

$S = \left| \frac{\rho g}{P_s} \cdot \frac{\partial V}{\partial \sigma} \right|$: vertical wind shear

$F_s(Ri)$: Stability dependent function

$Ri = -\frac{\rho g^2}{P_s} \cdot \left(\frac{1}{S^2} \cdot \frac{\partial \ln \theta_V}{\partial \sigma} \right)$: local Richardson number which is a function of the virtual potential temperature (θ_V) and acceleration of gravity (g).

$F_s(Ri)$ is defined as:

$$F_s(Ri) = (1 - 18 \cdot Ri)^{1/2} \quad (Ri < 0).$$

$$F_s(Ri) = 1 - \frac{Ri}{Ri_C} \qquad (0 < Ri < Ri_C = 0.2).$$

$F_s(Ri) = 0 \qquad (Ri > Ri_C = 0.2).$

A.2. Cumulus convection

The cumulus convection in the model is based on cumulus mass-fluxes calculated in a Kuo-Type scheme described in Grell et al. (1995). The model also includes entrainment and detrainment processes on convective updrafts and downdrafts in the form proposed by Tiedtke (1989). In the model, the convective rates are determined in the following steps:

1) The cloud base level σ_c is obtained by adding small perturbation humidity and temperature to levels below the σ level corresponding to 700 hPa and adiabatically lifting the air parcel until the condensation occurs. The cloud base σ_c is set to the lowest level where condensation would occur.

2) The supply rate of moisture available for penetrative convection is then estimated. The horizontal moisture divergence is evaluated from winds and water vapor content. Low-level moisture convergence M_l is obtained by integrating the horizontal moisture convergence below cloud base level:

$$M_l = -\left[\int_{\sigma_C}^{1} \nabla_\sigma (p_S \cdot \vec{V} \cdot q) d\sigma - M_C\right] + S_{evap}, \tag{A2}$$

where S_{evap} is surface evaporation. To account for deviation from the mass conservation in the wind data, the moisture divergence term is corrected for non-zero divergence of the air mass M_c:

$$M_C = \int_{\sigma_C}^{1} q \cdot \nabla_\sigma (p_S \cdot \vec{V}) d\sigma. \tag{A3}$$

Several criteria are checked to exclude grid cells with no significant deep cumulus convection following Grell et al. (1995).

3) The mass flux M_u in updraft is set to M_l divided by water vapour mixing ratio at cloud base q_{base}, so that $M_l=M_u\cdot q_{base}$. The vertical profiles of entrainment and detrainment rates are set to be proportional to M_u in accordance with Tiedtke (1989). In the updraft air, virtual potential temperatures are evaluated from the cloud base level to the cloud top level. The cloud top is determined by comparing the virtual potential temperatures in the updraft and environment, for which an overshot of 3 K is allowed.

4) The cloud with thickness of thinner than $\Delta\sigma=0.1$ are excluded. The downdraft mass flux is set 0.2 of that in the updraft, same as in Tiedtke (1989).

5) The tracers are transported vertically by applying a simplified explicit scheme. It is assumed that the updraft and downdraft make only a negligibly small part of a grid column; the rest is designated as environment air. First the vertical profiles of the concentrations in the updraft and downdraft air are computed by taking into account rates of mixing with environment air by entrainment and detrainment, and then the concentration tendencies in environment air are obtained from the entrainment/detrainment rates.

Appendix B

Model Performance in Simulating Atmospheric CO_2

Using the NIES transport model and the Biome-BGC biospheric flux model, the forward simulations for the case of daily varying Biome-BGC flux and the case of monthly varying Biome-BGC flux were done. Before comparing the difference between these two simulations at a series of CO_2 measurement sites, it is useful to show how the model simulated CO_2 concentrations compare with observations at the measurement sites. There are only a limited number of sites with continuous CO_2 concentration measurements necessary for this comparison in the period 1990-1999. In this section, a comparison of the two simulations to observations at three measurement sites representing the three different types of sites discussed in this study is presented. The three sites are Mauna Loa (a background site far from continental biospheric sources), Alert (a background site near the continent) and Fraserdale (a continental site). The observational data we have used are from two sources: Mauna Loa from NOAA/CMDL (National Oceanographic and Atmospheric Administration/Climate Monitoring and Diagnostics Laboratory, USA) (Thoning et al., 1989), Alert and Fraserdale from MSC (Meteorological Service of Canada) (Trivett and Higuchi, 1989; Higuchi et al., 2003).

Figure A1 shows the time series of simulated atmospheric CO_2 concentrations with the Biome-BGC monthly and daily CO_2 fluxes (corresponding to Reference and Synoptic cases) at Mauna Loa, Alert and Fraserdale along with the observational results. The modeled and observational results are detrended, by subtracting the long-term components through the digital filtering method (Nakazawa et al., 1997). The time series of the observations are composed of only measurements in the afternoon, when PBL is well developed and CO_2 signals are well-mixed inside the PBL. The modeled CO_2 concentrations capture the overall seasonal cycles. There is no significant difference of the modeled atmospheric CO_2 with daily and monthly fluxes at Mauna Loa and Alert, while there are notable differences between the two cases in the growing seasons at Fraserdale.

The model simulation result with the monthly biospheric fluxes shows less synoptic variability than that with the daily.

For a more quantitative comparison of how well the model can simulate the observed variability, the standard deviations (as the measure of variability) of the monthly CO_2 concentration for the two simulations and observations are computed. Then each month's standard deviations (SD) are averaged over 10 years (1990-1999) to minimize data problem such as missing data. Figure A2 shows the 10-year averaged monthly SDs of simulated and observed CO_2 concentration for Mauna Loa, Alert and Fraserdale.

For Mauna Loa, the SDs for the Reference and Synoptic cases are nearly equal and both SDs are similar to the SD for the observation. The model SDs are very slightly large than the SD of the observation in the winter, and smaller than the observation SD in August to October, capturing only about 50% of the observed variability.

For Alert, the SDs for the Reference and Synoptic cases are nearly equal in the winter. While in the growing season (June - October), the SD for the Synoptic case is about 10% larger than the Reference case. Comparing to the observation SD, the model SDs are too large in the winter and spring, up to ~200% larger in March. In the growing season, the observation SD is larger than the model SDs, as the model SDs can capture about 40-70% the observation SD. The large SD in the model CO_2 concentration appears to be caused by too much winter respiration signals.

Fraserdale results show much more difference between the Reference and Synoptic cases. In the winter (December, January, February), the model SDs are very similar to each other and both are larger than the observation SD (similar to Alert). Then from April to October, the Synoptic case SD is significantly larger than the Reference case SD. The Reference case SD is only about 50% as large as the Synoptic case SD between April to July. In August and September, the difference in the SDs is quite large, the Reference case is capturing only about 15-30% of the Synoptic case. The Synoptic SD appears to be much closer to the observation SD than the Reference SD.

These results show that the model can simulate the seasonal cycle reasonably at the different measurement sites. The variability is simulated better in the Synoptic case than the Reference case at the continental site. In this study, the difference between the Synoptic and Reference cases are examined in both forward and inverse modelling.

Reference

Andres, R. J., Marland, G. and Bischoff, S. 1996. Carbon dioxide emissions from fossil fuel combustion and cement manufacture 1751 – 1991 and an estimate of their isotopic composition and latitudinal distribution. In: *1993 Global Change Institute* (ed. T. Wigley and D. Schimel). Cambridge Univ. Press, New York, 419-429.

Baker, D. F., Law, R. M., Gurney, K. R., Rayner, P., Peylin, P., Denning, A. S., Bousquet, P., Bruhwiler, L., Chen, Y.-H., Ciais, P., Fung, I.Y., Heimann, M., John, J., Maki, T., Maksyutov, S., Masarie, K., Prather, M., Pak, B., Taguchi, S. and Zhu, Z. 2006. TransCom3 inversion intercomparison: Impact of transport model error on the interannual variability of regional CO_2 fluxes,1988-2003. *Global Biogeochem. Cycles* **20**, GB1002, doi:10.1029/2004GB002439.

Brenkert, A .L. 1998. Carbon dioxide emission estimates from fossil-fuel burning, hydraulic cement production, and gas flaring for 1995 on a one degree grid cell basis. NDP-058A, CDIAC, ORNL, Oak Ridge, Tenn., USA.

Chan, D., Yuen, C. W., Higuchi, K., Shashkov, A., Liu, J., Chen, J. and Worthy, D. 2004. On the CO_2 exchange between the atmosphere and the biosphere: The role of synoptic and mesoscale processes. *Tellus* **56B**, 194-212.

Denning, A. S., Fung, I. and Randall, D. 1995. Latitudinal gradient of atmospheric CO_2 due to seasonal exchange with land biota. *Nature* **376**, 240-243.

Denning, A. S., Collatz, J. G., Zhang, C., Randall, D. A., Berry, J. A., Sellers, P. J., Colello, G. D. and Dazlich, D. A. 1996a. Simulations of terrestrial carbon metabolism and atmospheric CO_2 in a general circulation model. Part 1: Surface carbon fluxes. *Tellus* **48B**, 521-542.

Denning, A. S., Randall, D. A., Collatz, G. J. and Sellers, P. J. 1996b. Simulations of terrestrial carbon metabolism and atmospheric CO_2 in a general circulation model. Part 2: Spatial and temporal variations of atmospheric CO_2. *Tellus* **48B**, 543-567.

Enting, I. G. 2002. *Inverse Problems in Atmospheric Constituent Transport*. Cambridge Univ. Press, New York.

Fujita, D., Ishizawa, M., Maksyutov, S., Thornton, P., Saeki, T. and Nakazawa, T. 2003. Inter-annual variability of the atmospheric carbon dioxide concentrations as simulated with global terrestrial biosphere models and atmospheric transport model. *Tellus* **55B**, 530-546.

GLOBALVIEW-CO_2. 2000. Cooperative Atmospheric Data Integration Project-Carbon Dioxide [CD-ROM], NOAA Clim. Model. And Diag. Lab., Boulder, Colo., USA.

Grell, G., Dudhia, J. and Stauffer, D. 1995. Description of the Fifth-Generation Penn State/NCAR Mesoscale Model (MM5), NCAR/TN-398. NCAR, Boulder, Colo., USA.

Gurney, K., Law, R., Rayner, P. and Denning. A. S. 2000. TransCom 3 Experimental Protocol. Department of Atmospheric Science, Colorado State University, USA. Paper No. 707. (Available at http://transcom.colostate.edu/TransCom_3/transcom_3.html)

Gurney, K. R., Law, R. M., Denning, A. S., Rayner, P. J., Baker, D., Bousquet, P., Bruhwiler, L., Chen, Y.-H., Ciais, P., Fan, S., Fung, I. Y., Gloor, M., Heimann, M., Higuchi, K., John, J., Maki, T., Maksyutov, S., Masarie, K., Peylin, P., Prather, M., Pak, B. C., Randerson, J., Sarmiento, J., Taguchi, S., Takahashi, T. and Yuen. C. W. 2002. Towards robust regional estimates of CO_2 sources and sinks using atmospheric transport models. *Nature* **415**, 626-630.

Gurney, K. R., Law, R. M., Denning, A. S., Rayner, P. J., Pak, B. C., Baker, D., Bousquet, P., Bruhwiler, L., Chen, Y.-H., Ciais, P., Fung, I. Y., Heimann, M., John, J., Maki, T., Maksyutov, S., Peylin, P., Prather, M. and Taguchi. S. 2004. Transcom 3 inversion intercomparison: Model mean results for the estimation of seasonal carbon sources and sinks. *Global Biogeochem. Cycles* **18**, GB1010, doi:10.1029/2003/GB002111.

Gurney, K. R., Chen, Y.-H., Maki, T., Kawa, S. R., Andrews, A. and Zhu Z. 2005. Sensitivity of atmospheric CO_2 inversinos to seasonal and interannual variations in fossil fuel emissions. *J. Geophys. Res*., **110** D10308, doi:10.1029/2004JD005373.

Hack, J. J., Boville, B. A., Briegleb, B. P., Kiehl, J. T., Rasch, P. J. and Williamson, D. L. 1993. Description of the NCAR community climate model (CCM2), NCAR/TN-382, NCAR, Boulder, Colo., USA.

Higuchi, K., Worthy, D. E. J., Chan D. and Shashkov, A. 2003. Regional source/sink impact on the diurnal, seasonal and inter-annual variations in atmospheric CO_2 at a boreal forest site in Canada. *Tellus* **55B**, 115- 125.

Kalnay, E., Kanamitsu, M., Kistler, R., Collins, W., Deaven, D., Gandin, L., Iredell, M., Saha, S., White, G., Woollen, J., Zhu, Y., Chelliah, M., Ebisuzaki, W., Higgins, W., Janowiak, J., Mo, K. C., Ropelewski, C., Wang, J., Leetmaa, A., Reynolds, R., Jenne, R. and Joseph, D. 1996. The NCEP/NCAR 40-year reanalysis project. *Bulletin of the American Meteorological Society* **77**, 437-471.

Maksyutov S. and Inoue, G. 2000. Vertical profiles of radon and CO_2 simulated by the global atmospheric transport model. In: *CGER Supercomputer activity report*, *I039-2000* **7**, CGER NIES, Tsukuba, Japan, 39-41.

Nakazawa, T., Ishizawa, M., Higuchi, K. and Trivett, N. B. A. 1997. Two curve fitting methods applied to CO_2 flask data. *Environmetrics*, **8**, 197-218.

Randerson, J. T., Matthew, M. V., Conway, T. J, Fung, I. Y. and Field, C. B. 1997. The contribution of terrestrial sources and sinks to trends in the seasonal cycles of atmospheric carbon dioxide. *Global Biogeochem. Cycles* **11**, 553-560.

Rayner, P. J., Enting, I. G., Francey, R. J. and Langenfelds R. 1999. Reconstructing the recent carbon cycle from atmospheric CO_2, ^{13}C and O_2/N_2 observations. *Tellus* **51B**, 213-232.

Takahashi, T., Wanninkhof, R. H., Feely, R. A., Weiss, R. F., Chipman, D. W., Bates, N., Olafsson, J., Sabine, C. and Sutherland, S. C. 1999. Net sea-air CO_2 flux over the global oceans: An improved estimate based on the sea-air pCO_2 difference. In: *Proceedings of the 2nd International Symposium: CO_2 in the Oceans* (ed. Y. Nojiri). Tsukuba, Japan.

Tarantola, A. 1987. *Inverse Problem Theory: Methods for Data Fitting and Model Parameter Estimation*. Elsevier Sci., New York.

Thornton, P. E., Law, B. E., Gholz, H. L., Clark, K.L., Falge, E., Ellsworth, D. S., Goldstein, A. H., Monson, R. K., Hollinger, D., Falk, M., Chen, J., Sparks, J. P. 2002. Modeling and measuring the effects of disturbance history and climate on carbon and water budgets in evergreen needleleaf forests. *Agric. For. Meteorol.* **113**, 185-222.

Thoning, K.W., Tans, P. P. and Komhyr, W. D. 1989. Atmospheric carbon dioxide at Mauna Loa Observatory, 2. Analysis of the NOAA/GMCC data, 1974-1985., *J. Geophys. Res.* ,**94**, 8549-8565.

Tiedtke, M. 1989. A comprehensive mass flux scheme for cumulus parameterization in large-scale models, *Mon. Wea. Rev.*, **117**, 1779-1800.

Trivett, N. B. A. and Higuchi, K. 1989. Trends and seasonal cycles of atmospheric CO_2 over Alert, Sable Island, and Cape St. James, as analyzed by forward stepwise regression technique. pp. 27-42. In: *The Statistical Treatment of CO_2 Data Records* (ed. W.P. Elliott). Air Resources Laboratory, Silver Spring, Maryland, USA.

Table 1. Observation sites selected for this study

Index in Fig. 1	Site	Country	Latitude [º]	Longitude [º]	Altitude [m]
Background: remote sites					
a	Mauna Loa	U.S.A.	19.53 N	155.58 W	3397
b	Cape Grim	Australia	40.68 S	144.68 E	94
Background: coastal sites					
c	Alert	Canada	82.45 N	62.52 W	210
d	Estevan Point	Canada	49.38 N	126.55 W	500
e	Sable Island	Canada	43.93 N	60.02 W	5
f	Ryori	Japan	39.03 N	141.83 E	260
Continental					
g	Fraserdale	Canada	49.88 N	81.57 W	250
h	Hegyhatsal	Hungary	46.95 N	16.65 E	258

Table 2. The global land, ocean and total (land + ocean) inverse flux estimates for 1992-1995 for the Reference, Synoptic and their difference (GtC yr^{-1})

Year	Reference Inversion			Synoptic Inversion			Difference (Syn. – Ref.)		
	Land	Ocean	Total	Land	Ocean	Total	Land	Ocean	Total
1992	-2.00	-2.81	-4.81	-2.11	-2.58	-4.69	-0.11	0.23	0.12
1993	-2.02	-1.28	-3.30	-2.45	-0.80	-3.25	-0.44	0.48	0.04
1994	0.73	-2.68	-1.95	0.59	-2.45	-1.86	-0.14	0.23	0.09
1995	1.03	-3.31	-2.28	0.94	-3.06	-2.12	-0.09	0.25	0.16

The annual uncertainties have very minor variations during these years; the uncertainties are ±1.5 GtC yr^{-1} and ±0.5 GtC yr^{-1} for the global land and ocean respectively. The uncertainties are similar for both the Reference and Synoptic cases.

Table 3. The between-methods differences of flux estimate and the mean posterior uncertainties in the reference and synoptic inversions (GtC yr^{-1})

	Between-methods difference (this study)	Mean posterior uncertainty (this study)	"Between" Uncertainty (Gurney et al., 2004)	"Within" Uncertainty (Gurney et al., 2004)
Land Regions				
Boreal North America	0.80	0.27	0.28	0.18
Temperate North America	0.73	0.24	0.32	0.22
Tropical America	1.20	0.61	0.77	0.73
South America	0.64	0.60	0.61	0.64
Tropical Africa	0.79	0.53	0.85	0.54
South Africa	0.84	0.66	0.60	0.58
Boreal Asia	1.02	0.33	0.51	0.23
Temperate Asia	1.02	0.36	0.74	0.34
Tropical Asia	0.89	0.43	0.94	0.45
Australia	0.23	0.13	0.15	0.14
Europe	1.65	0.24	0.43	0.18
Ocean Regions				
North Pacific	0.49	0.19	0.28	0.14
Tropical West Pacific	0.31	0.14	0.27	0.15
Tropical East Pacific	0.20	0.15	0.27	0.18
South Pacific	0.58	0.18	0.49	0.29
Northern Ocean	0.58	0.12	0.17	0.08
North Atlantic	0.36	0.16	0.30	0.15
Tropical Atlantic	0.14	0.13	0.16	0.18
South Atlantic	0.19	0.15	0.07	0.24
Southern Ocean	0.28	0.19	0.33	0.17
Tropical Indian Ocean	0.23	0.19	0.26	0.19
South Indian Ocean	0.12	0.17	0.22	0.19

The between-methods differences are the root mean square of monthly flux estimate differences between the reference and synoptic inversions. For comparison, "Between-model" and "Within-model" Uncertainties from the seasonal inversion study of TransCom 3 Level 2 (Gurney et al., 2004) are listed.

Figure Captions

Figure 1. Locations of the sites where the time series of CO_2 concentration are discussed ((a)Mauna Loa, (b)Cape Grim, (c)Alert, (d)Estevan Point, (e)Sable Island, (f) Ryori,(g)Fraserdale and (h)Hegyhatsal), and the 11 land and 11 ocean regions for the inversion. The site descriptions are listed in Table 1.

Figure 2. The 10-year time evolution of the monthly average CO_2 concentration difference (Synoptic – Reference) at various locations. Mauna Loa and Cape Grim are remote sites. Alert, Estevan Point, Sable Island and Ryori are coastal sites. Fraserdale and Hegyhatsal are continental sites.

Figure 3. The global distribution of the monthly average CO_2 concentration difference (Synoptic – Reference) for each month of 1992.

Figure 4. The global distribution of the annually average CO_2 concentration difference (Synoptic – Reference) for the year 1992 (a) and 1993 (b).

Figure 5. The estimated monthly fluxes for the 11 land regions by the Reference (black line) and Synoptic inversions (black dotted line). A negative flux indicates uptake of CO_2 by the land. Also shown is the prior flux from the neutral biosphere (gray line).

Figure 6. The estimated monthly fluxes for the 11 ocean regions by the Reference (black line) and Synoptic inversions (black dotted line). A negative flux indicates uptake of CO_2 by the ocean. Also shown is the prior flux from the ocean (gray line).

Figure 7. The estimated annual fluxes for the 11 land regions by the Reference (black line) and Synoptic inversions (black dotted line). A negative flux indicates uptake of CO_2 by the land.

Figure 8. The estimated annual fluxes for the 11 ocean regions by the Reference (black line) and Synoptic inversions (black dotted line). A negative flux indicates uptake of CO_2 by the ocean.

Figure 9. The time series of detrended atmospheric CO_2 concentrations simulated with the Biome-BGC monthly and daily CO_2 fluxes (corresponding to Reference and Synoptic cases, respectively) at Mauna Loa, Alert and Fraserdale, along with the observations.

Figure 10. The 10-year averaged monthly standard deviations of simulated atmospheric CO_2 concentrations at Mauna Loa, Alert and Fraserdale for Reference and Synoptic cases, along with the observations.

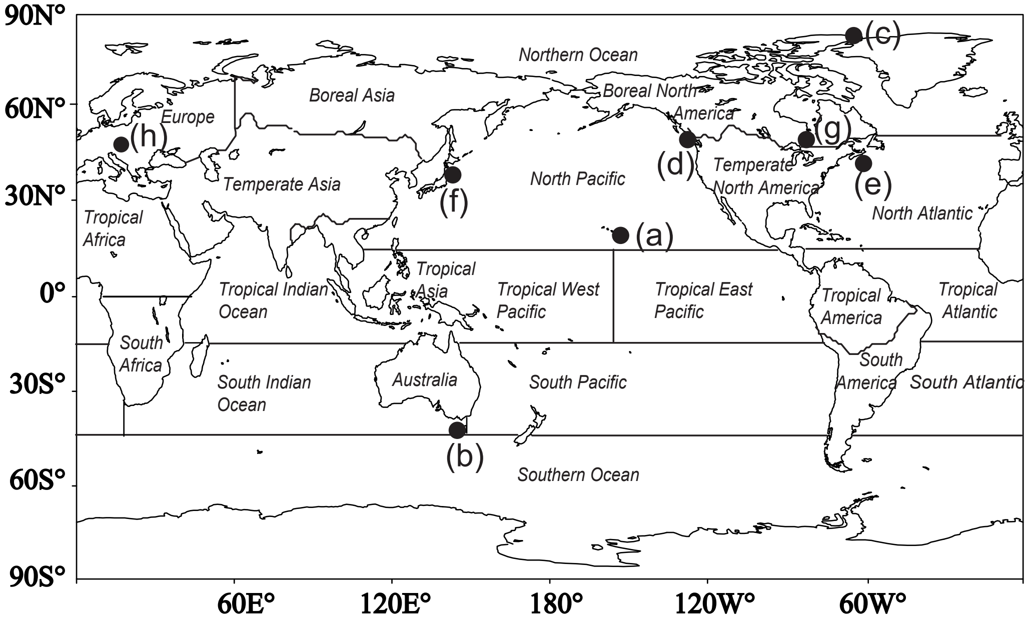
90N°
60N°
30N°
0°
30S°
60S°
90S°
60E°
120E°
180°
120W°
60W°
(a)
(b)
(c)
(d)
(e)
(f)
(g)
(h)
Northern Ocean
Boreal Asia
Europe
Boreal North America
Temperate Asia
North Pacific
Temperate North America
North Atlantic
Tropical Africa
Tropical Indian Ocean
Tropical Asia
Tropical West Pacific
Tropical East Pacific
Tropical America
Tropical Atlantic
South Africa
South Indian Ocean
Australia
South Pacific
South America
South Atlantic
Southern Ocean

Fig. 1

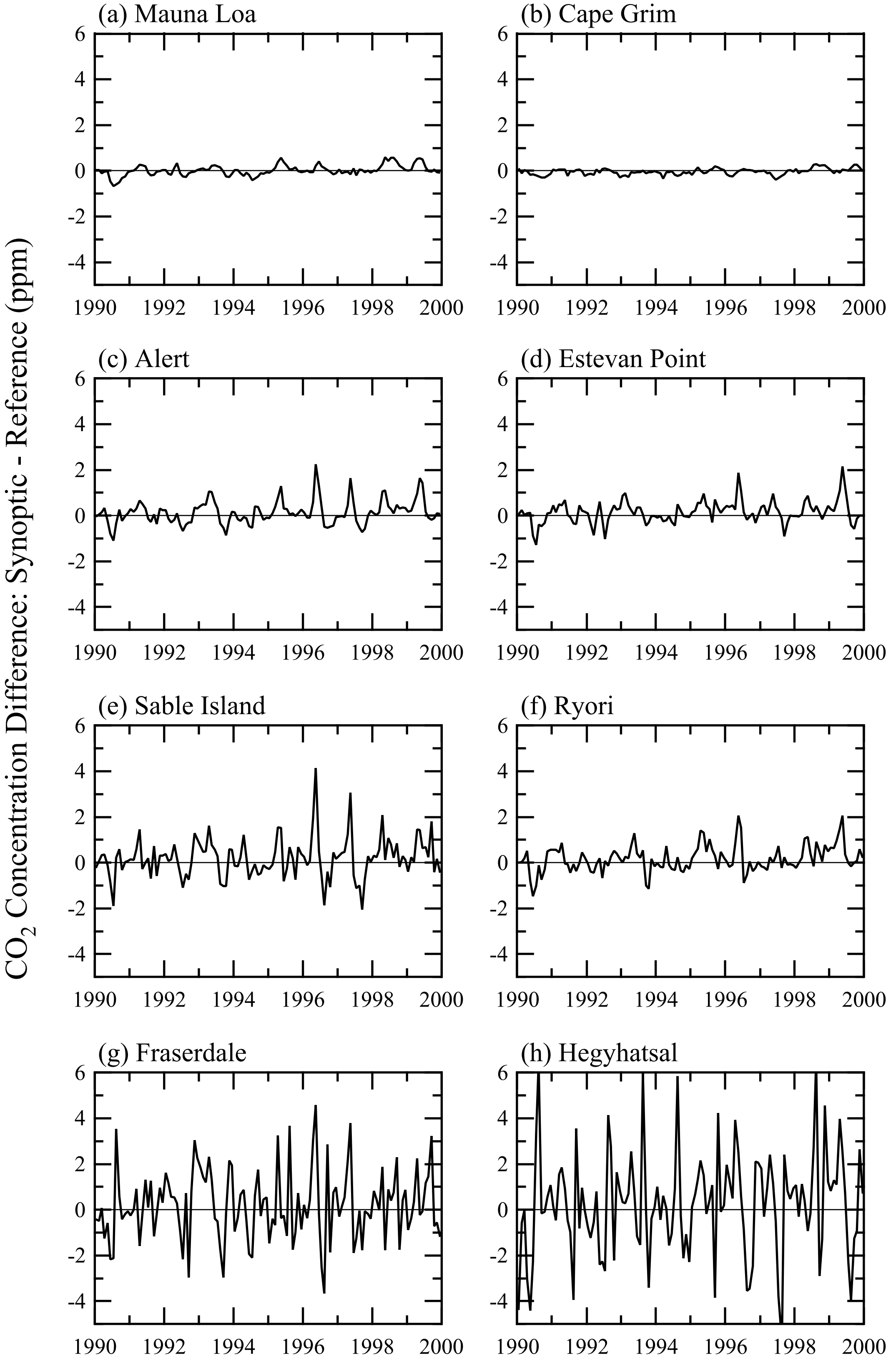
(a) Mauna Loa
(b) Cape Grim
(c) Alert
(d) Estevan Point
(e) Sable Island
(f) Ryori
(g) Fraserdale
(h) Hegyhatsal
CO_2 Concentration Difference: Synoptic - Reference (ppm)
6
4
2
0
-2
-4
1990
1992
1994
1996
1998
2000

Fig. 2

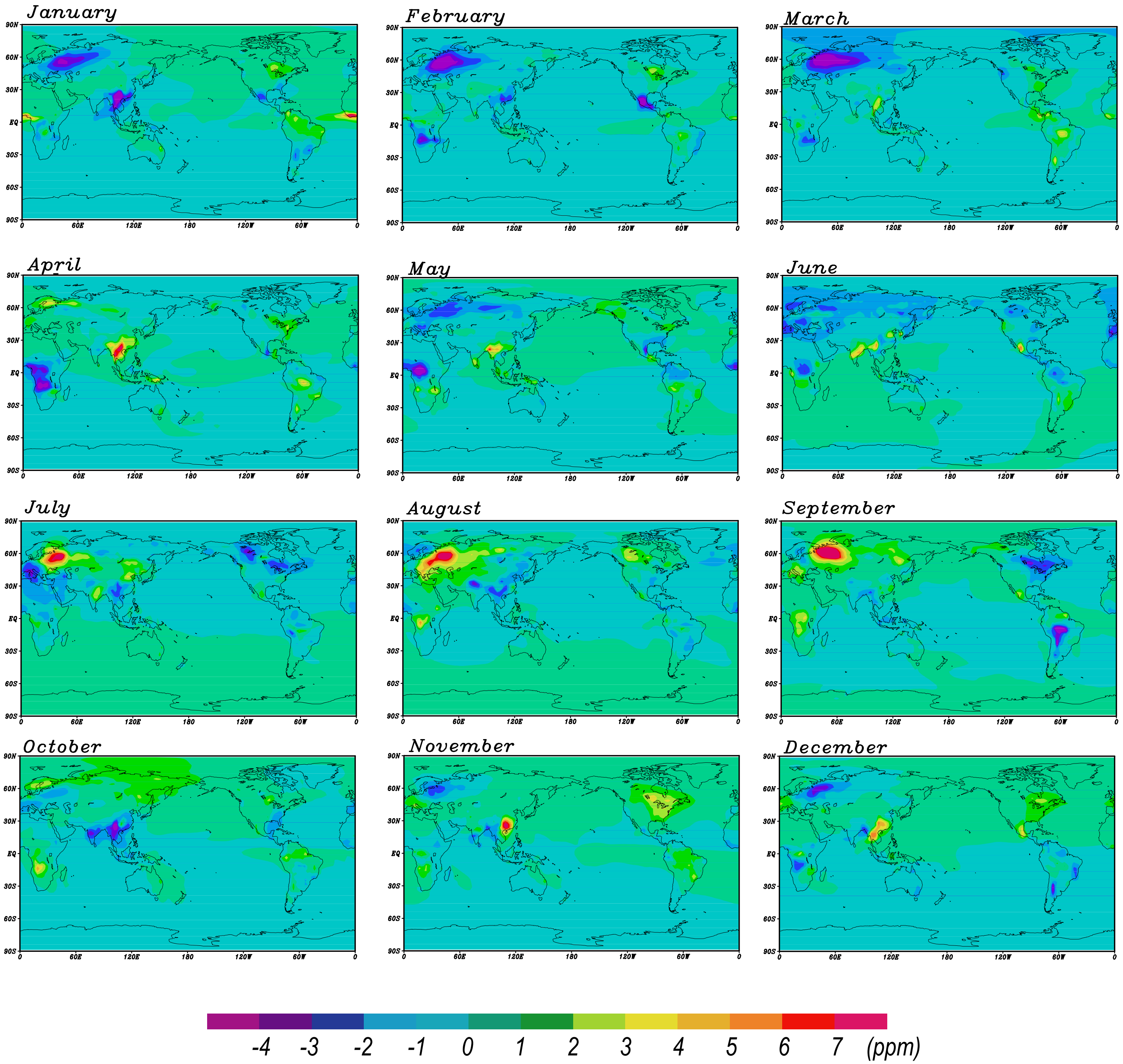
January
February
March
April
May
June
July
August
September
October
November
December
90N
60N
30N
EQ
30S
60S
90S
0
60E
120E
180
120W
60W
0
-4
-3
-2
-1
0
1
2
3
4
5
6
7
(ppm)

Fig. 3

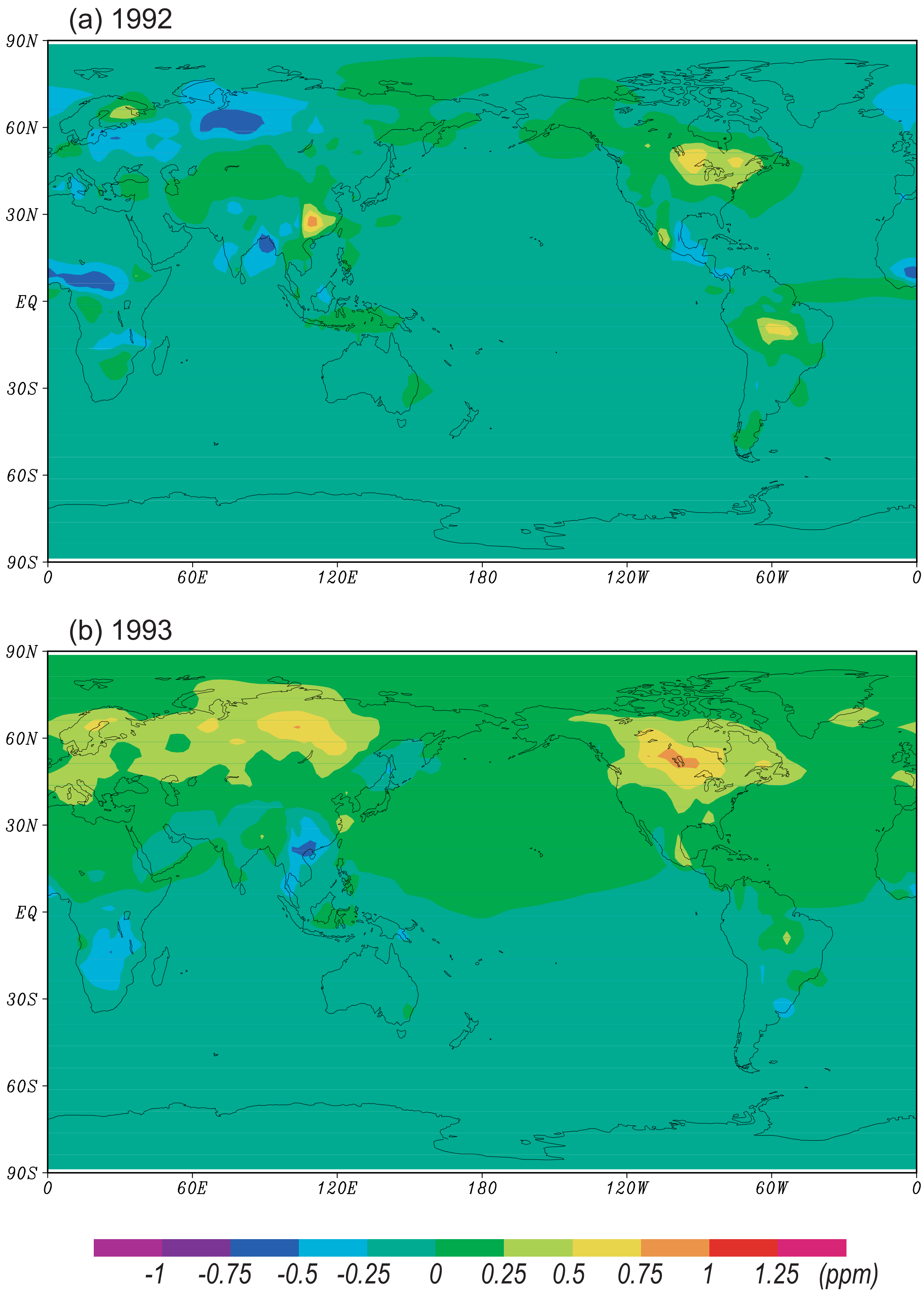
(a) 1992
90N
60N
30N
EQ
30S
60S
90S
0
60E
120E
180
120W
60W
0
(b) 1993
90N
60N
30N
EQ
30S
60S
90S
0
60E
120E
180
120W
60W
0
-1
-0.75
-0.5
-0.25
0
0.25
0.5
0.75
1
1.25
(ppm)

Fig. 4

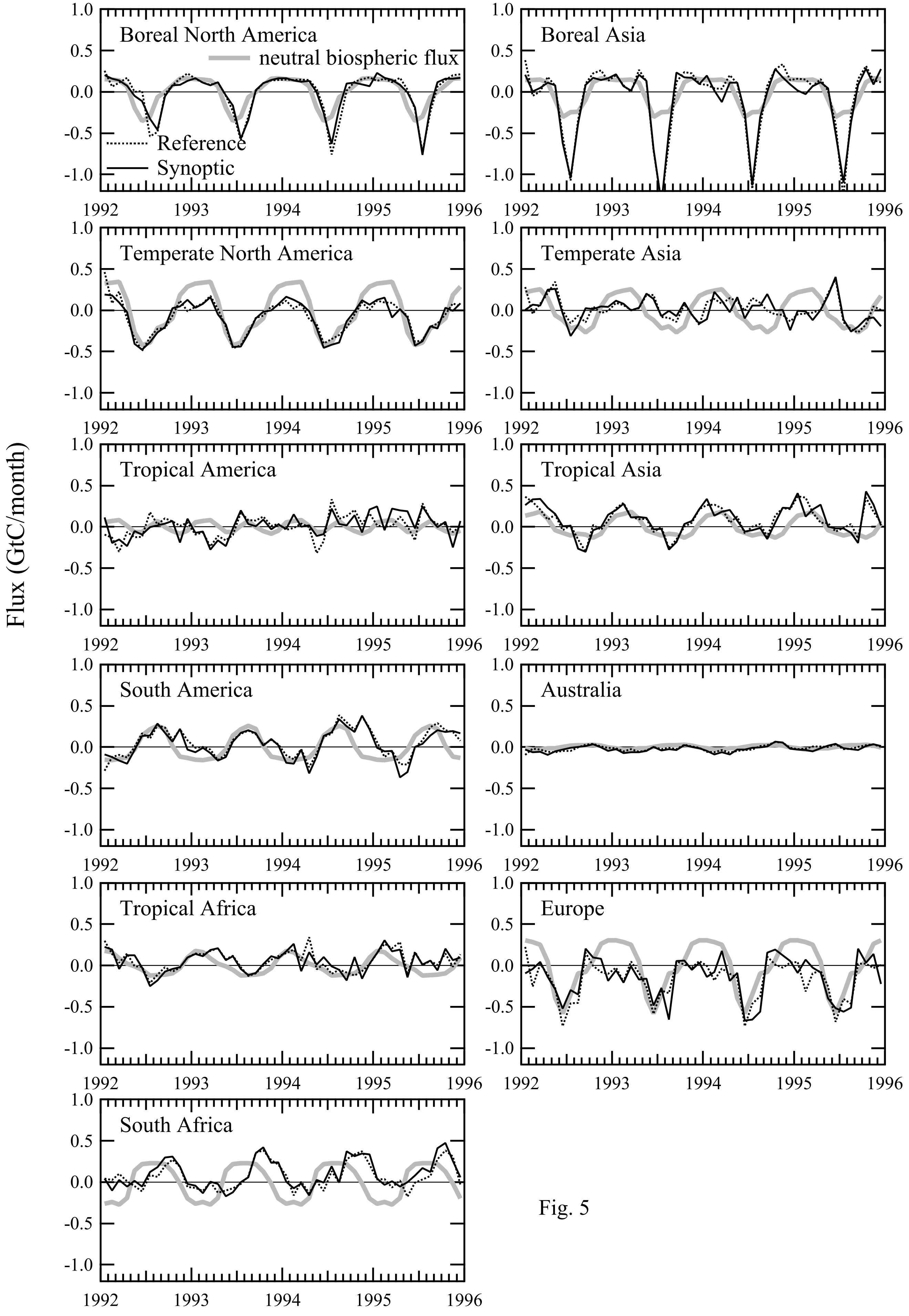
Flux (GtC/month)
Boreal North America
neutral biospheric flux
Reference
Synoptic
Boreal Asia
Temperate North America
Temperate Asia
Tropical America
Tropical Asia
South America
Australia
Tropical Africa
Europe
South Africa
1.0
0.5
0.0
-0.5
-1.0
1992
1993
1994
1995
1996

Fig. 5

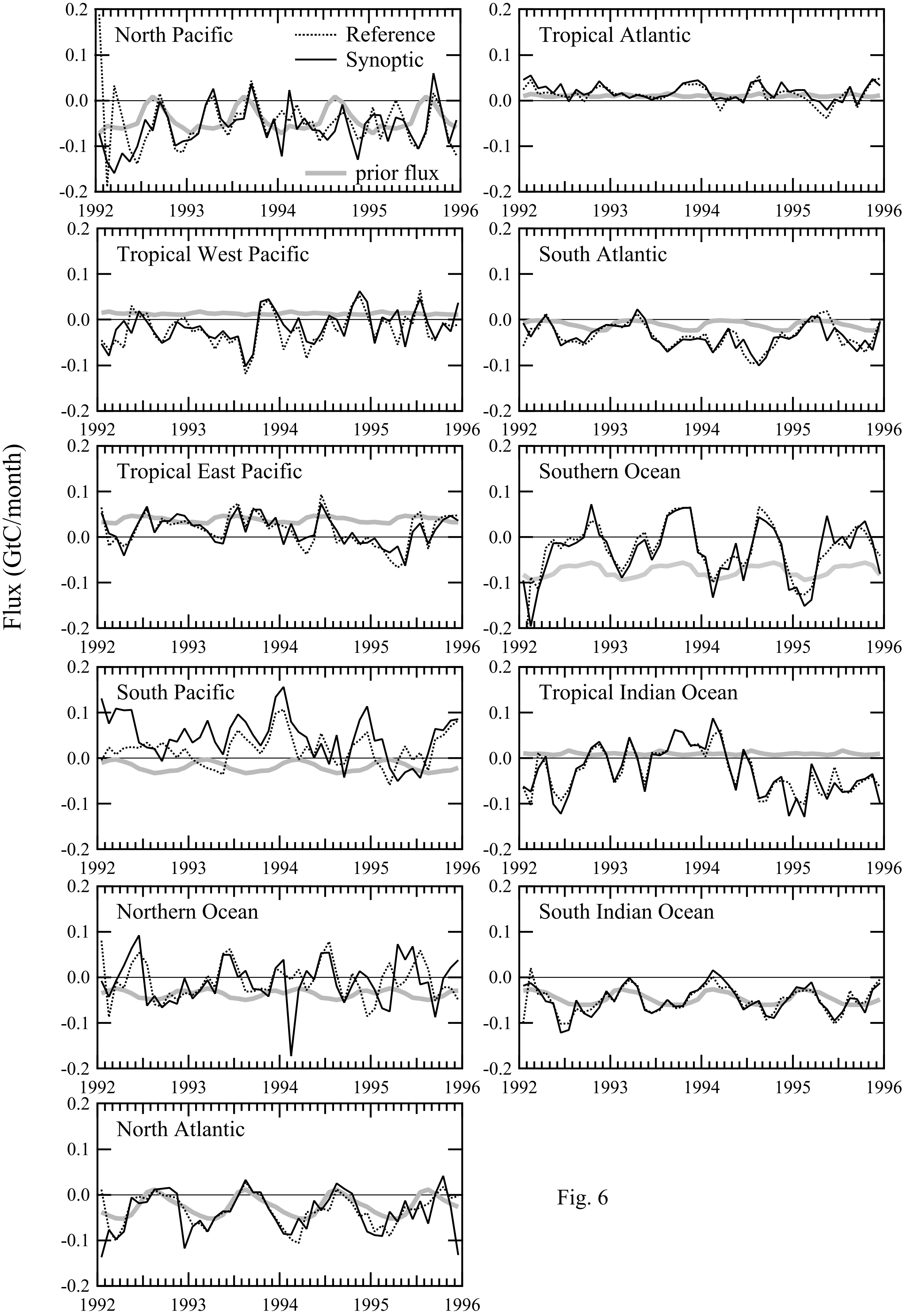
Flux (GtC/month)
North Pacific
Reference
Synoptic
prior flux
Tropical Atlantic
Tropical West Pacific
South Atlantic
Tropical East Pacific
Southern Ocean
South Pacific
Tropical Indian Ocean
Northern Ocean
South Indian Ocean
North Atlantic
0.2
0.1
0.0
-0.1
-0.2
1992
1993
1994
1995
1996

Fig. 6

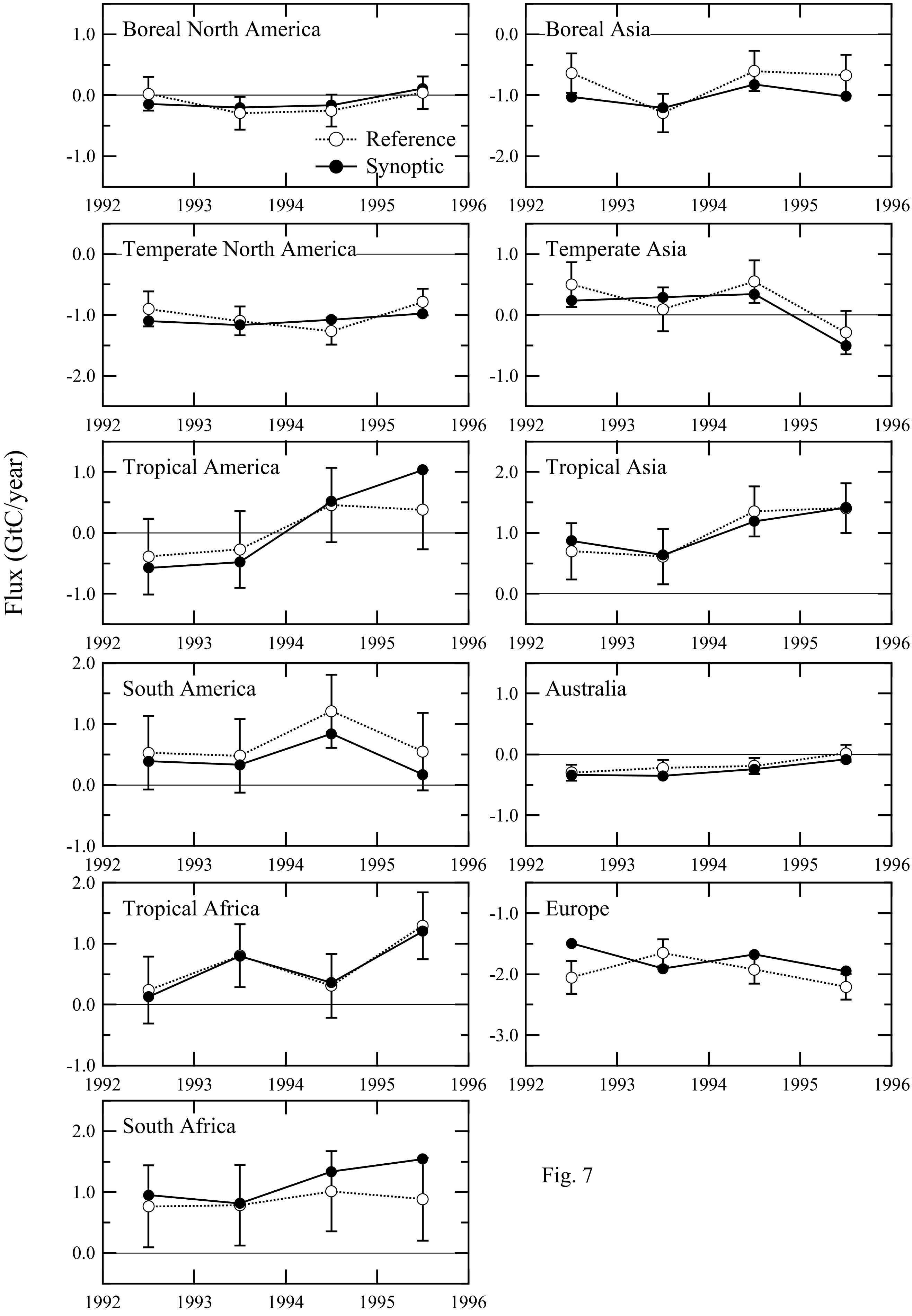
Flux (GtC/year)
Boreal North America
Reference
Synoptic
Boreal Asia
Temperate North America
Temperate Asia
Tropical America
Tropical Asia
South America
Australia
Tropical Africa
Europe
South Africa
1992
1993
1994
1995
1996
-3.0
-2.0
-1.0
0.0
1.0
2.0

Fig. 7

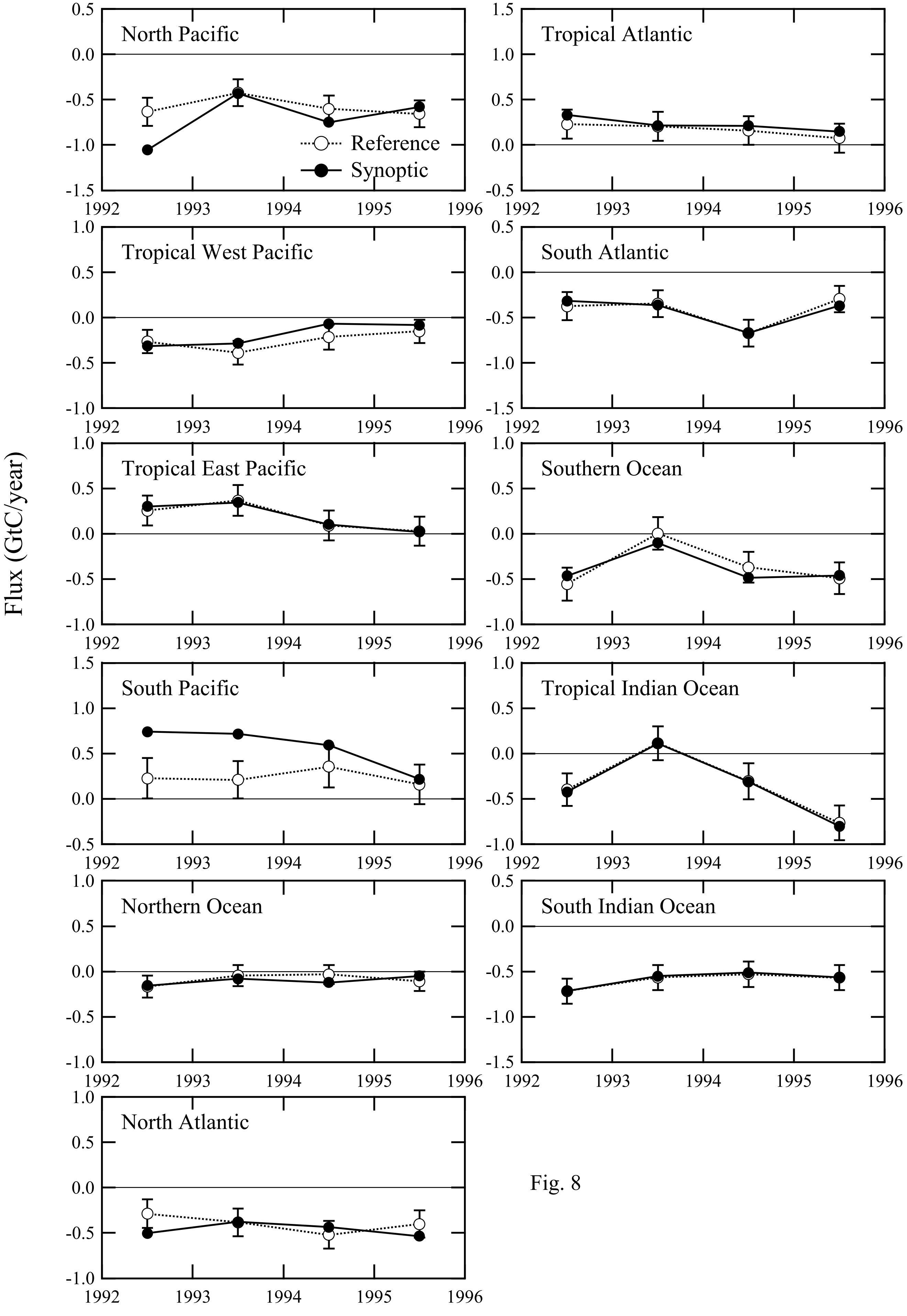
Flux (GtC/year)
North Pacific
Reference
Synoptic
Tropical Atlantic
Tropical West Pacific
South Atlantic
Tropical East Pacific
Southern Ocean
South Pacific
Tropical Indian Ocean
Northern Ocean
South Indian Ocean
North Atlantic
1992
1993
1994
1995
1996
1.5
1.0
0.5
0.0
-0.5
-1.0
-1.5

Fig. 8

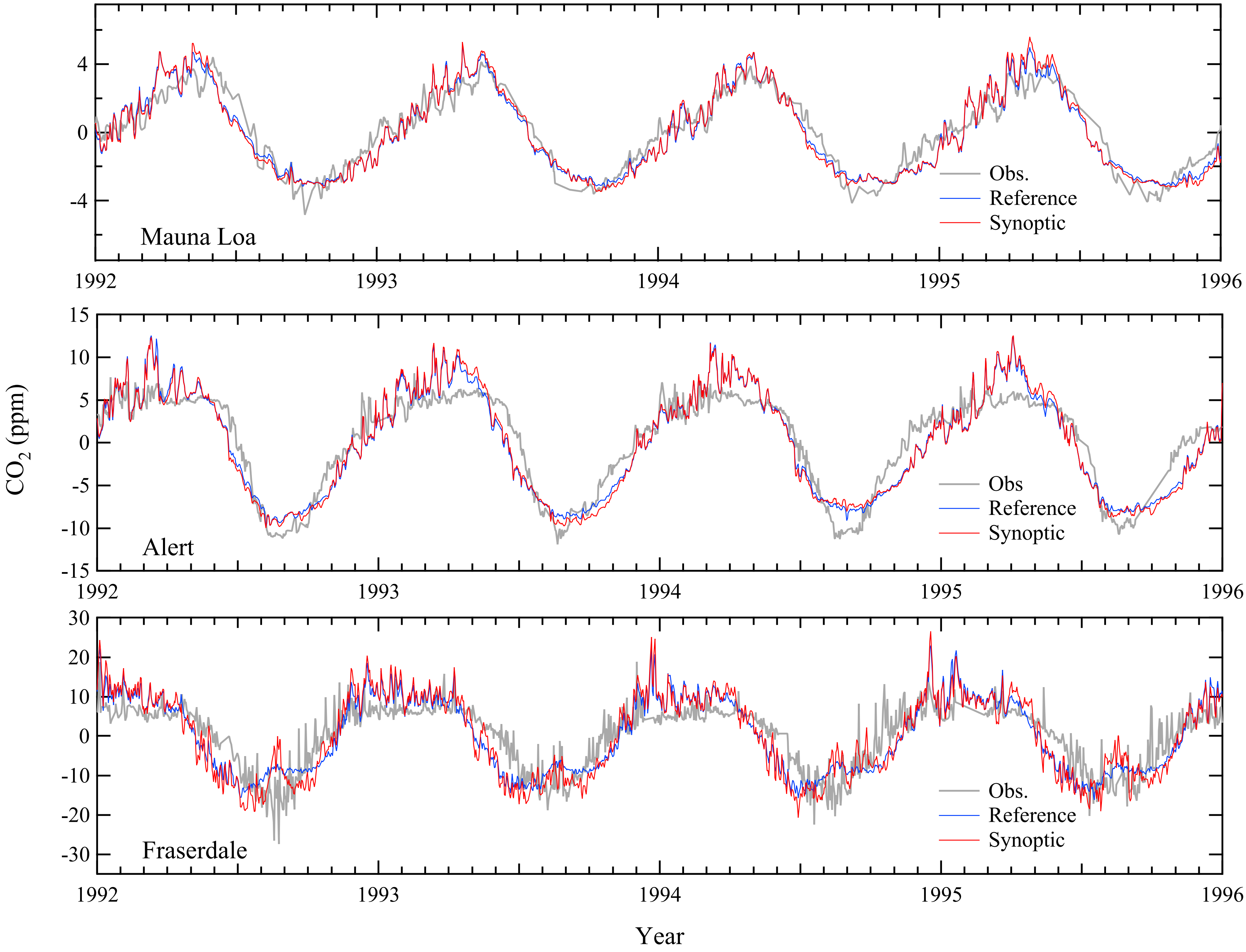
Mauna Loa
Alert
Fraserdale
Obs.
Obs
Reference
Synoptic
CO$_2$ (ppm)
Year
4
0
-4
15
10
5
0
-5
-10
-15
30
20
10
0
-10
-20
-30
1992
1993
1994
1995
1996

Fig. 9

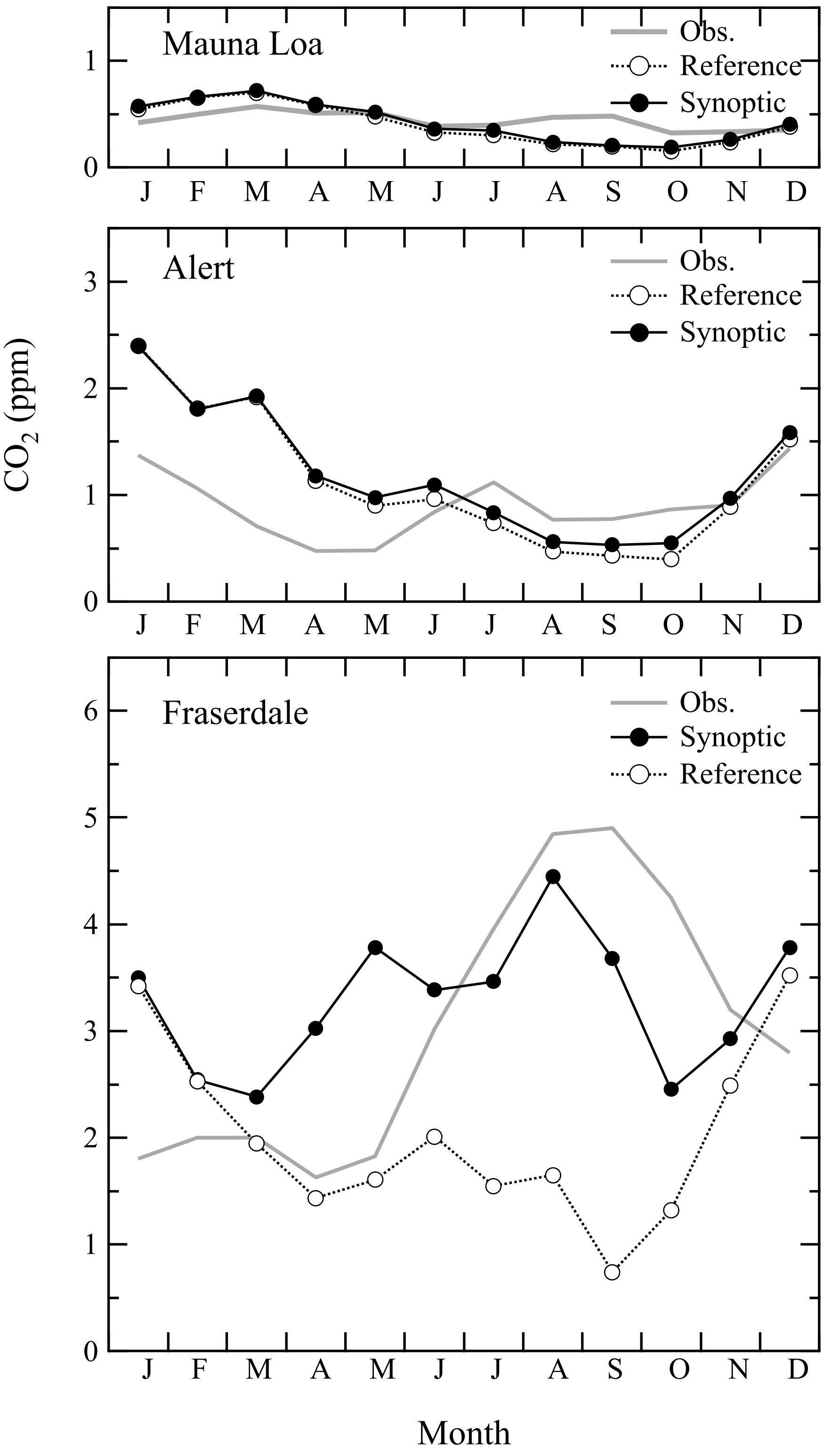
Mauna Loa
Obs.
Reference
Synoptic
1
0
J
F
M
A
M
J
J
A
S
O
N
D
Alert
Obs.
Reference
Synoptic
3
2
1
0
Fraserdale
Obs.
Synoptic
Reference
6
5
4
3
2
1
0
CO$_2$ (ppm)
Month

Fig. 10